INVITED PAPER Special Section on Electronic Displays

Improved Resolution Enhancement Technique for Broadband Illumination in Flat Panel Display Lithography

Kanji SUZUKI[†a)] ***and*** **Manabu HAKKO**[†], ***Nonmembers***

SUMMARY In flat panel display (FPD) lithography, a high resolution and large depth of focus (DOF) are required. The demands for high throughput have necessitated the use of large glass plates and exposure areas, thereby increasing focal unevenness and reducing process latitude. Thus, a large DOF is needed, particularly for high-resolution lithography. To manufacture future high-definition displays, 1.0 μm line and space (L/S) is predicted to be required, and a technique to achieve this resolution with adequate DOF is necessary. To improve the resolution and DOF, resolution enhancement techniques (RETs) have been introduced. RETs such as off-axis illumination (OAI) and phase-shift masks (PSMs) have been widely used in semiconductor lithography, which utilizes narrowband illumination. To effectively use RETs in FPD lithography, modification for broadband illumination is required because FPD lithography utilizes such illumination as exposure light. However, thus far, RETs for broadband illumination have not been studied. This study aimed to develop techniques to achieve 1.0 μm L/S resolution with an acceptable DOF. To this end, this paper proposes a method that combines our previously developed RET, namely, divided spectrum illumination (DSI), with an attenuated PSM (Att. PSM). Theoretical observations and simulations present the design of a PSM for broadband illumination. The transmittance and phase shift, whose degree varies according to the wavelength, are determined in terms of aerial image contrast and resist loss. The design of DSI for an Att. PSM is also discussed considering image contrast, DOF, and illumination intensity. Finally, the exposure results of 1.0 μm L/S using DSI and PSM techniques are shown, demonstrating that a PSM greatly improves the resist profile, and DSI enhances the DOF by approximately 30% compared to conventional OAI. Thus, DSI and PSMs can be used in practical applications for achieving 1.0 μm L/S with sufficient DOF.

key words: *lithography, resolution enhancement technique, off-axis illumination, phase-shift mask, broadband illumination*

1. Introduction

Optical lithography is an important fine patterning method in the display and semiconductor manufacturing industries [1], [2]. With the increase in demand for high-productivity and high-definition patterning, exposure tools have improved in terms of resolution and throughput. For flat panel display (FPD) lithography, the size of glass plates for mass production of display panels has been enlarged to achieve high productivity, primarily by developing manufacturing techniques for large optical elements, aberration correction systems across a wide exposure area, and high-power illumination optical systems.

Exposure tools in FPD manufacturing can be categorized as follows: multi-lens optical systems [3] and mirror optical systems [4]–[6]. Figure 1 shows the structure of Canon's exposure systems, which use a mirror optical system for projection optics. Illuminated light from the illumination optics irradiates a mask, thereby copying mask features onto the plate below. Employing mirror elements for projection optics allows using broadband illumination as exposure light because mirror elements, in principle, do not exhibit chromatic aberration. Using broadband illumination is one of the most efficient solutions for achieving high productivity in FPD manufacturing.

The minimum line width—often referred to as the critical dimension (CD)—should be small to form high-density circuits. Here, the CD represents the resolution of the exposure tools. The depth of focus (DOF)—representing the focal length that can maintain image contrast—is also an important factor. In the lithographic process, there is unevenness in the focal direction, which is produced by mask flatness, glass plate flatness, vibration of stages, or the field curvature of the projection optics. These focus errors decrease the process latitude, which hampers CD control. It is particularly difficult to attain CD control in small CD processes. Consequently, a large DOF is required.

However, there is a trade-off between resolution and DOF, as expressed by the Rayleigh equation [7]:

$$\mathrm{CD} = k_1 \frac{\lambda}{\mathrm{NA}} \tag{1}$$

$$\mathrm{DOF} = k_2 \frac{\lambda}{\mathrm{NA}^2} \tag{2}$$

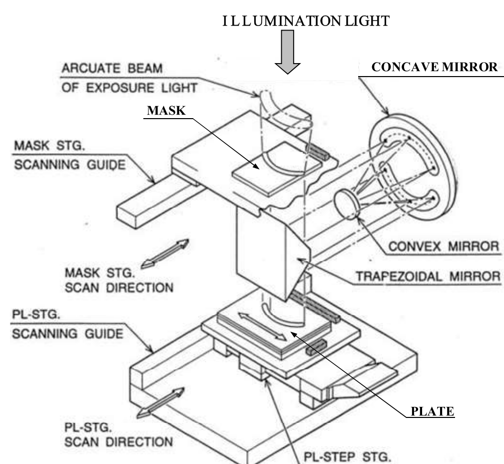

Fig. 1 Configuration of a mirror-projection exposure system.

Manuscript received March 15, 2021.
Manuscript publicized August 17, 2021.
[†]The authors are with Optical Products Operations, Flat Panel Display Production Equipment PLM Center 4, Canon Inc., Utsunomiya-shi, 321–3292 Japan.
a) E-mail: suzuki.kanji@mail.canon
DOI: 10.1587/transele.2021DII0004

Copyright © 2022 The Institute of Electronics, Information and Communication Engineers

where k_1 and k_2 are constants related to the process conditions, λ is the wavelength of the exposure light, and NA is the numerical aperture of the exposure tool. Resolution can be improved by shortening the exposure wavelength and enlarging the NA, both of which decrease the DOF. To improve the resolution by minimizing the decrease in DOF, shortening the wavelength is better than enlarging the NA as the NA^2 term significantly decreases the DOF.

Recently, we developed a new high-resolution technique to use deep ultraviolet (DUV) broadband exposure light, instead of the conventional ghi-line light [8]. By shortening the exposure wavelength, high-resolution patterning of a 1.2 μm line and space (L/S) pattern can be achieved. With the continuous performance improvement of display devices, the need for higher resolutions is expected to remain. Some researchers have reported that next-generation smartphones and head-mount displays will require circuit patterns with a CD of 1.0 μm [9], [10].

To achieve higher resolutions, a phase-shift mask (PSM) can be used. Previously, we showed that DUV exposure with a PSM could resolve an L/S pattern of 1.0 μm [11]. However, it was also revealed that the DOF for a 1.0 μm L/S pattern decreased compared to that of patterns with a wider pitch. The DOF for a 1.2 μm L/S pattern with a binary intensity mask (BIM) was 24.3 μm, while that for a 1.0 μm L/S pattern with a PSM was 19.5 μm. To maintain sufficient process latitude, the DOF must be improved to the same extent as that of the 1.2 μm L/S pattern.

Previously, we developed a resolution enhancement technique (RET), named divided spectrum illumination (DSI), which is suitable for FPD lithography using broadband exposure light [12]. The current study aimed to develop a technique to achieve 1.0 μm L/S resolution with adequate DOF. To this end, we investigated the combination of DSI and PSM using theoretical observations, simulations, and experiments. In particular, the design of a PSM for broadband illumination and the use of DSI in conjunction with a PSM are discussed in detail.

2. Divided Spectrum Illumination (DSI)

This section describes the principle and design method of DSI. First, the problems associated with conventional illumination techniques used in FPD lithography are reviewed.

2.1 Off-Axis Illumination (OAI)

The off-axis illumination, such as dipole, quadrupole, and annular illumination, has contributed to the improvement of the resolution and DOF in fine patterning lithographic processes [13]–[17]. In conventional illumination, a mask is irradiated via perpendicular incident (on-axis) and oblique incident (off-axis) light. In OAI techniques, the light that is perpendicular to the plane of incidence is cut off, thus illuminating a mask with only oblique (off-axis) light.

The resolution enhancement mechanism of OAI is as follows. Here, we assume that a mask feature is a periodic pattern that generates discrete diffraction order light. When a mask feature is so small that the first-order diffraction angle exceeds the numerical aperture of the projection optics, the first-order diffraction light of perpendicular incident light is not captured by the optical system, resulting in no image formation and degradation of image contrast. However, oblique incident light may prevent this situation. By manipulating the incident angle so that both the zero- and first-order light can be gathered by the optical system, the illumination light can aid image formation. This imaging system of interference with only two lights is referred to as two-beam imaging. OAI can be interpreted as employing an illumination source that selectively utilizes effective light for two-beam imaging and excludes undesirable light that induce image degradation.

DOF enhancement of OAI can be described as a decrease in the phase difference between the diffraction orders. Defocusing creates a phase error, whose degree is proportional to the square of the position at the pupil. When the angle of incident light is tuned such that the zero- and first-order light can be symmetrically positioned with respect to the optical axis at the pupil, the phase difference can be reduced and the image degradation due to defocusing minimized. In other words, the DOF can be improved. This condition can be expressed as follows [18]:

$$\sigma_c = \frac{\lambda}{2\mathrm{NA}\cdot P} \tag{3}$$

where σ_c is the optimized illumination angle (normalized using the NA), λ is the wavelength of the exposure light, NA is the numerical aperture of the projection optics, and P is the pitch of the exposed pattern. Note that the optimum illumination conditions vary based on the wavelength and pattern pitch.

Although OAI has been used primarily in the field of semiconductor lithography, this technique has recently been applied in FPD lithography [8]. Figure 2 shows the exemplary OAI shape used in FPD lithography. An annular source is the most popular OAI shape because efficient off-axis illumination can be obtained for L/S patterns in arbitrary directions. Here, its radius σ is defined as $(f_x^2 + f_y^2)^{1/2}$, where f_x and f_y are the illumination angles in the x- and y-directions, respectively, normalized using the NA. In conventional OAI for FPD lithography, the entire spectrum of broadband exposure light is used throughout the source area.

To the best of our knowledge, OAI has not been optimized for broadband illumination. In general, semiconduc-

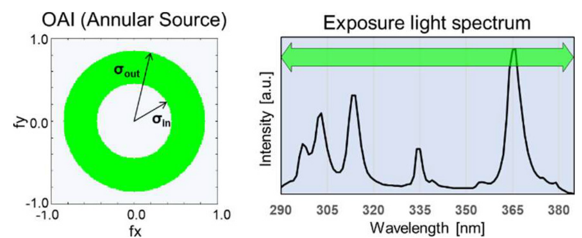

Fig. 2 Example of conventional OAI for FPD lithography.

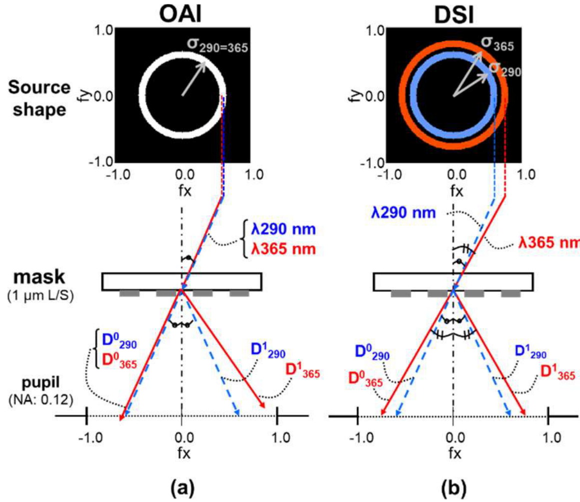

Fig. 3 Illustration of light paths in (a) OAI and (b) DSI for λ = 290 and 365 nm.

tor lithography utilizes narrowband exposure light, whereas FPDs utilize broadband exposure light. In semiconductor lithography, the exposure light has practically a single wavelength, and the illumination angle of the OAI is clearly defined by Eq. (3). Exposure light in FPD lithography, however, has a wide range of wavelengths, which results in deviations from Eq. (3), based on the wavelength. Figure 3 (a) depicts OAI systems with illumination wavelengths of 290 and 365 nm. For each wavelength, the transmission (zero order) and diffraction light (first order) paths are shown. Conventional OAI uses the same σ region, $\sigma_{290=365}$, without distinction between the two wavelengths. However, the diffraction angle varies depending on wavelengths in principle. When a specific wavelength light is optimized to satisfy the condition of symmetrical propagation (290 nm case), the other wavelength light does not propagate symmetrically (365 nm case). Therefore, the DOF is not effectively improved by conventional OAI for broadband illumination.

2.2 Divided Spectrum Illumination (DSI)

The key concept of DSI is illumination wavelength optimization based on the illumination angle. Figure 3 (b) shows the DSI systems under the same conditions as Fig. 3 (a). DSI uses different σ regions (σ_{290} and σ_{365}) based on the wavelength so that each light wavelength satisfies the optimum illumination condition of Eq. (3). Consequently, the phase difference between diffraction orders is reduced, and high image contrast with defocusing can be obtained for both 290 nm and 365 nm illumination.

A DSI design based solely on Eq. (3) is not optimal because excessive tuning of the illumination source may cause two problems: low illumination intensity and high pattern-pitch-dependence. When DSI is formed by cutting off all light, which slightly deviates from Eq. (3), the light intensity decreases considerably compared to that of conventional OAI. In terms of illumination intensity, as much

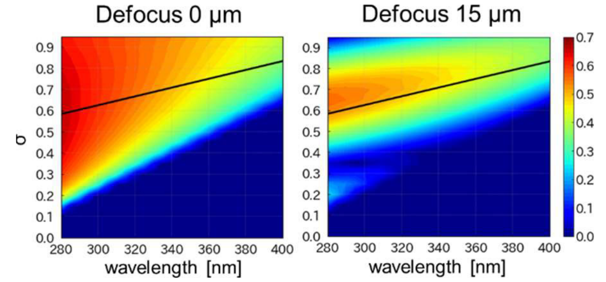

Fig. 4 Aerial image contrast simulations with wavelength and σ variation (BIM, defocus = 0, 15 μm).

light as possible should be used for illumination. In addition, an illumination source strictly tuned for a specific pattern pitch exhibits poor performance for the other pitches. This can be explained using Eq. (3), where the optimum illumination conditions depend on the pattern pitch. Masks for product manufacturing contain various features, and thus, illumination with low pattern-pitch-dependence is desirable. Therefore, the illumination source should not follow Eq. (3) solely but should also be tuned based on illumination intensity, robustness to pattern-pitch dependence, and image contrast calculation for desired source shape.

The illumination condition to achieve large DOF is understood using Fig. 4, wherein the two-dimensional plot of the aerial image contrasts with the wavelength (horizontal axis) and illumination angle (vertical axis) variance for a BIM with the focus states of 0 and 15 μm. An exposure L/S pattern had a CD of 1.0 μm, with a pitch of 2.0 μm, and the NA was 0.12. Hereinafter, we assume the pattern to have a 1.0 μm L/S and a NA of 0.12, unless otherwise noted. Ultra-narrow annular illumination with an annulus width of σ = 0.05 was used, and the vertical coordinate in Fig. 4 corresponds to its inner σ. The black solid line in Fig. 4 corresponds to the condition that satisfies Eq. (3). At its best focus, high contrast was achieved in the region where the ratio of illumination lights contributing to image formation is large (i.e., large η, described later). In the 15 μm defocus case, image contrast was degraded, except for the region corresponding to Eq. (3). The slight deviation of the high-contrast region from the solid black line results from the difference between small radius dipole and annular illumination [12]. To obtain a large DOF, the illumination conditions that induce large contrast degradation with defocusing should be filtered out. However, the cut-off region should be minimized to maintain sufficient illumination intensity and robustness for pattern-pitch dependence, i.e., the DSI should be designed to balance these conflicting demands.

Figure 5 shows the DSI design, which has two source areas: a source area with σ = 0.65–0.85 and a wavelength region of 290–385 nm (WR1), and an area with σ = 0.45–0.65 and a wavelength region of 290–350 nm (WR2). The inner σ (σ_{in}), boundary σ (σ_{bo}), and outer σ (σ_{out}) are 0.45, 0.65, and 0.85, respectively. These parameters eliminate the i-line, which corresponds to the wavelength region of 350–

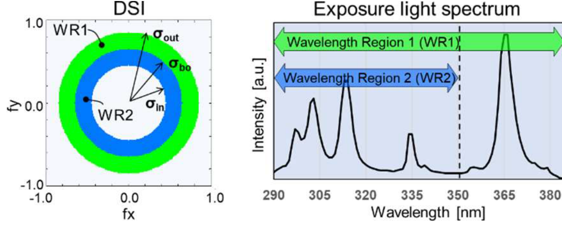

Fig. 5 DSI design for 1.0 µm L/S (σ_{in} = 0.45, σ_{bo} = 0.65, and σ_{out} = 0.85). The region of σ = 0.45–0.65 corresponds to the WR2 (loss of i-line), whereas the region of σ = 0.65–0.85 corresponds to the WR1 (the whole spectrum).

385 nm, near the inner σ region from 0.45–0.65. As described later, the DOF is not maximized for σ_{bo} = 0.65. However, we ignored the slight decrease in the DOF for increasing illumination intensity.

3. Phase-Shift Mask for Broadband Illumination

This section describes the design of a PSM for broadband illumination and a DSI design in combination with a PSM.

3.1 Attenuated Phase-Shift Mask (Att. PSM)

A PSM is a RET used to improve aerial image contrast on a plate by modulating the phase of illumination light. There are two types of PSM: alternating PSM (Alt. PSM) [19], [20] and attenuated PSM (Att. PSM) [21], [22]. The latter is extensively used in semiconductor manufacturing because of its ease of manufacture and defect inspection [23]. An Att. PSM consists of a phase-shifting film, where MoSi is extensively used in the Cr region of a BIM [24]. The light passing through the phase-shifting film undergoes a phase shift of 180° (π) and light intensity attenuation. The destructive interference between phase-shifted background light and non-phase-shifted diffraction light improves the contrast of the image intensity on the image plane.

The amount of phase shift and transmittance of the phase-shifting film varies based on wavelength, which is problematic in broadband illumination. In narrow band illumination, this wavelength dependence is inconsequential, and the phase shift of π and the attenuation of light intensity should simply be configured to a single wavelength. Conversely, in broadband illumination, the phase-shifting of a precise π can be obtained at a specific wavelength, while phase errors from π occur for the other wavelengths. Consequently, the impact of phase errors and transmittance changes should be examined, and a design method for a PSM for broadband illumination established. Details of the PSM design for contact-hole patterning with broadband illumination can be found in our previous work [25].

3.2 Design of PSM for Broadband Illumination

To investigate the PSM design for an L/S pattern with broadband illumination, we first describe how the PSM parameters affect the image intensity of an L/S pattern. Second, the impact of the transmittance is examined. Finally, the impact of the phase error from π is discussed.

Assuming an equivalent L/S pattern (its pitch P is twice its CD) arranged in the x-direction is illuminated by lights whose illumination angles are symmetrical in the x-direction with two-beam image formation, the image intensity $I(x)$ is given by [26].

$$I(x) = |a_0|^2 + \eta|a_1|^2 + 2\eta|a_0||a_1|\cos(\Delta\psi_{1-0})\cos(2\pi x/P) \quad (4)$$

$$a_0 = (1 + te^{i\phi})/2 \quad (5)$$

$$a_1 = (1 - te^{i\phi})/\pi \quad (6)$$

where a_0 and a_1 are the amplitudes of zero- and first-order amplitudes, ϕ is the degree of phase shift, t is the amplitude transmittance of the phase-shifting film, η is the ratio of two-beam imaging, and $\Delta\psi_{1-0}$ is the phase difference between the zero- and first-order light. η represents the ratio of illumination light, which is effective for two-beam imaging, while $1 - \eta$ represents the ratio of no image formation. The ratio η for annular illumination can be theoretically calculated as a function of the wavelength, annular radius, NA, and pattern pitch [27]. The phase difference $\Delta\psi_{1-0}$ is derived from the phase error of a PSM and defocusing. In the partially coherent illumination case, the total image intensity is calculated using the weighted average of Eq. (4) for different illumination angles and wavelengths.

Next, the impact of the transmittance change is examined based on these equations. Figure 6 (a) illustrates the image contrast with transmittance and the ratio of the two-beam imaging variance, calculated using the weighted average of Eq. (4), assuming no phase difference ($\Delta\psi_{1-0} = 0$). In the case of near-ideal two-beam imaging ($\eta \approx 1$), the peak of the image contrast is at a transmittance of 6%, which is the typical transmittance of an Att. PSM. In the assumed imaging system with an annular source of σ = 0.45–0.85, the ratio η is 0.3–0.6 over the wavelength range of 290–385 nm (see Fig. 6 (b)). In this region, the transmittance of the contrast peak becomes greater than 6%, although the transmittance dependency of the image contrast becomes relatively weak. The intensity transmittance difference over the broadband spectrum was approximately 0.1, where a drastic change in the image contrast did not occur. Thus, it can be concluded that the transmittance change over the illumination spectrum is inconsequential, and the transmittance value of the centroid wavelength can be considered to represent that of the entire spectrum.

In determining the transmittance of a PSM, resist loss should also be considered, which is induced by high transmittance and leads to patterning defects. To measure this impact, resist simulations were conducted using PROLITH (KLA Corp, Milpitas, CA, USA) simulation software [28]. The simulation results are shown in Fig. 7—the plot of the aerial image contrast (solid line) and the resist loss (dotted line) as a function of the intensity transmittance. The exposure wavelength was 340 nm, which was the centroid wavelength of the DUV spectrum. The pattern for contrast

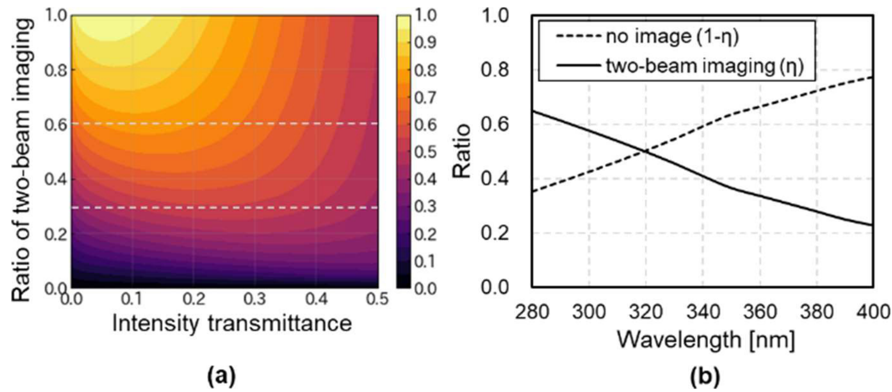

Fig. 6 (a) Calculated image contrasts with the transmittance and ratio of 2-beam imaging variance, (b) the ratio of 2-beam imaging with wavelengths for P = 2000 nm, NA = 0.12, and the illumination source of σ = 0.45–0.85.

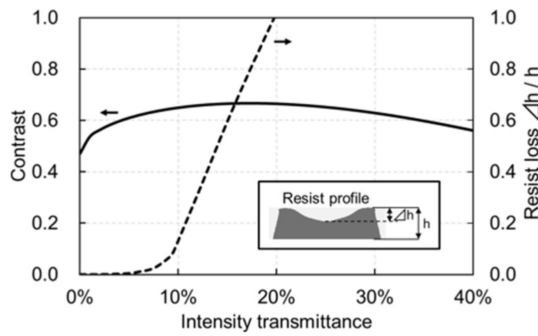

Fig. 7 Simulation results for aerial image contrast for 1.0 µm L/S (the solid line) and resist loss for 10 µm L/S (the dotted line) with intensity transmittance variance.

evaluation was 1.0 µm L/S, while that for resist loss evaluation was 10 µm L/S, where the maximum resist loss was observed. The resist loss was evaluated to be the loss height Δh relative to the resist thickness h. The image contrast gradually increased as the transmittance increased, reaching a maximum at 17%. When the contrast threshold was set to 0.6, where a sharp resist profile was obtained, the transmittance range was 5–35%. By contrast, the resist loss for the broad pattern rapidly increased from 10%. To avoid large resist losses, the transmittance should be lower than 10%. Thus, the intensity transmittance of the phase-shifting film was determined in the range of 5–10%.

Next, we describe the impact of the phase error. When the phase error $\Delta\phi$ occurs ($\phi = \pi + \Delta\phi$), the phase difference $\Delta\alpha$ between zero- and first-order light is [29]

$$\Delta\alpha \approx \frac{2\Delta\phi t}{1 - t^2} \tag{7}$$

This approximate equation is established when $\Delta\phi$ is relatively small. Similarly, the focus error induces a phase difference $\Delta\beta$ from zero- to first-order light, and this difference is expressed as

$$\Delta\beta \approx -\frac{2\pi\delta NA}{P}\Delta\sigma \tag{8}$$

where δ is the distance from the focal plane (defocus), P is the pitch of an exposed pattern, and $\Delta\sigma$ is the sigma variance from σ_c defined by Eq. (3). The approximation is effective when the illumination angle is relatively small. Consequently, the phase difference $\Delta\psi_{1-0}$ in Eq. (4) is

$$\Delta\psi_{1-0} = \Delta\alpha + \Delta\beta = \frac{2\Delta\phi t}{1 - t^2} - \frac{2\pi\delta NA}{P}\Delta\sigma \tag{9}$$

Because the cosine of the phase difference $\Delta\psi_{1-0}$ causes image degradation, the difference should be zero so that the cosine term is maximized. Thus, $\Delta\phi$ of zero is desirable in the no-defocus case.

Assuming that the phase-shifting film is a single-layer structure of refractive index n and film thickness d, the phase error $\Delta\phi$ can be expressed as follows:

$$\Delta\phi = \frac{2\pi d(n-1)}{\lambda} - \pi = \frac{\pi(\lambda_{180} - \lambda)}{\lambda} \tag{10}$$

where λ_{180} represents the wavelength of π phase shift. This equation clearly indicates that phase error occurs at all wavelengths except for λ_{180}.

To quantify the above-mentioned perspectives, the calculated aerial image contrast with the wavelength and phase error $\Delta\phi$ variance for an annular illumination source of σ = 0.45–0.85 is shown in Fig. 8. The blue dotted line corresponds to the wavelength dependence of the phase error $\Delta\phi$ for λ_{180} of 340 nm, whereas the red dotted line indicates the case with no phase error over the range of wavelengths (i.e., ideal case). The image contrast decreases as the phase error increases, indicating that $\Delta\phi$ should be minimized for image contrast. However, the phase error is not zero, except for λ_{180}. Because the total image intensity is the weighted average over the whole spectrum, the image contrast with phase error (real case) is expected to be lower than that without phase error (ideal case) and vary depending on λ_{180}.

The resultant total image contrast with λ_{180} variance for the cases with and without phase error is shown in Fig. 9, where the intensity weight of the DUV spectrum is considered. It is evident that the phase error degraded the image contrast. The image contrast in the case with phase error gradually changes with λ_{180} variance and is maximized at

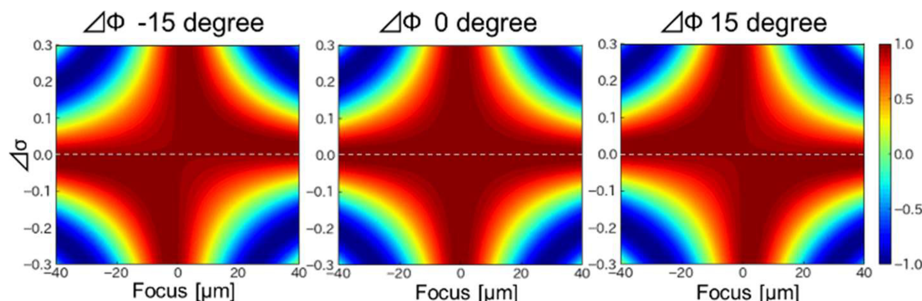

Fig. 10 Calculation results for the cosine term of phase differences.

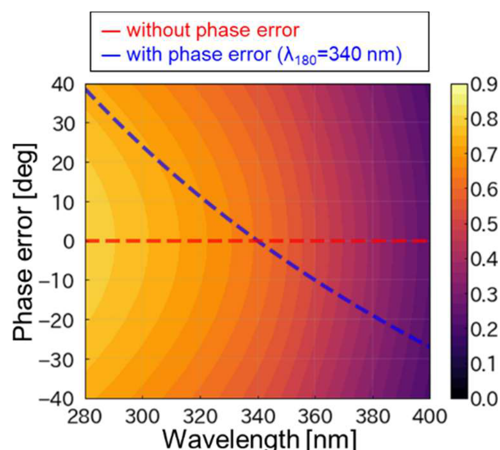

Fig. 8 Simulation results for aerial image contrast with wavelength and phase error variance.

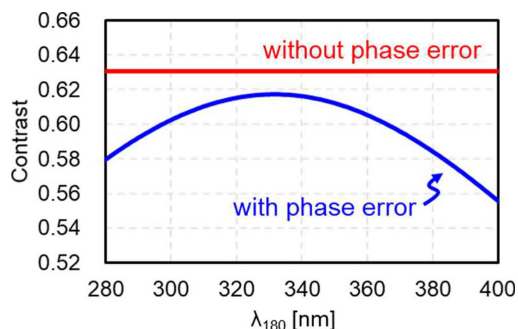

Fig. 9 Aerial image contrast with varying wavelength of π phase-shifting.

approximately 335 nm. Based on the contrast threshold of 0.6, λ_{180} can be in the range of 300–365 nm. Consequently, we determined λ_{180} to be 340 nm, the centroid wavelength of the DUV spectrum.

3.3 DSI Design with PSM

In this section, we discuss the DSI design in combination with a PSM. Particularly, it is important to determine whether the DSI design for a PSM is the same as that for a BIM. The deviation from the DSI condition of Eq. (3) appears as $\Delta\sigma$ in Eq. (9). When the phase error $\Delta\psi_{1-0}$ is zero, the cosine term in Eq. (3) is maximized, resulting in the maximum contrast. Thus, when the phase error $\Delta\phi$ is zero, $\Delta\sigma$ should be zero so that the phase difference $\Delta\psi_{1-0}$ is zero, which corresponds to the DSI condition. In contrast, when both the phase error $\Delta\phi$ and the defocus δ are nonzero, $\Delta\sigma$ should be configured such that $\Delta\psi_{1-0}$ is zero. Thus, the optimum illumination condition may vary from Eq. (3). Figure 10 shows the calculation results of $\cos(\Delta\psi_{1-0})$, with varying defocus δ and sigma difference $\Delta\sigma$. The phase error $\Delta\phi$ was −15, 0, 15° and the amplitude transmittance t was $\sqrt{0.06}$ (intensity transmittance of 6%). These results show that the phase difference of a PSM slightly changes the best illumination condition in the defocus case. However, the sign of $\Delta\sigma$ varies depending on the defocus direction, and thus $\Delta\sigma$ should be zero so that the contrast change with defocusing is unaffected by the direction of the defocus. Consequently, the optimized illumination condition for a BIM, Eq. (3), can also be applied to a PSM, i.e., the DSI designed for a BIM could be adopted for a PSM.

To confirm the above-mentioned prediction, resist simulations were conducted for a BIM and PSM by varying the boundary sigma σ_{bo} of DSI and fixing σ_{in} and σ_{out} to 0.45, and 0.85, respectively. The source region between σ_{in} and σ_{bo} corresponds to a WR2 of 290–350 nm, while that between σ_{bo} and σ_{out} (WR1) was 290–385 nm (Fig. 5). Here, the sources for σ_{bo} of 0.45 and 0.85 correspond to conventional OAI, while that of 0.85 differs from that of 0.45 in the point of loss of the i-line. As evident in Fig. 11 (a), the image contrast of a PSM is consistently greater than that of a BIM, indicating that a PSM can effectively improve the resolution. Figure 11 (b) reveals that the best condition for the DOF is the same for both mask types. Although the DOF is maximized at σ_{bo} = 0.75, the difference from that at σ_{bo} = 0.65, is small enough to be ignored (a decrease of 1–2%). Conversely, the illumination intensity decreases with an increase in σ_{bo} (i.e., the increase in the i-line cutoff), as shown in Fig. 11 (c). As σ_{bo} increases from 0.65 to 0.75, the intensity decreases by 11%, which is so large that the difference cannot be ignored. Therefore, we determined the DSI design for both mask types to be σ_{bo} = 0.65. Thus, the DSI design of a PSM was the same as that of a BIM in this case. However, this conclusion should not be overgeneralized, and the design parameters for a PSM should be carefully examined based on the illumination spectrum and the target pattern.

Mask	BIM		PSM	
Illumination source	OAI	DSI	OAI	DSI
Source shape				
Resist DOF [μm]	17.1	20.7	19.5	25.1
SEM image (x20k)				

Fig. 12 Experimental results for a 1.0 μm L/S pattern with a PSM.

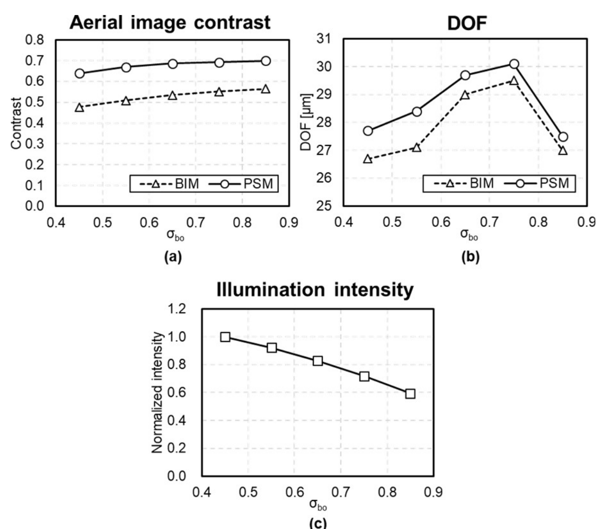

Fig. 11 Simulation results for (a) aerial image contrast, (b) DOF with a BIM and a PSM, and (c) illumination intensity normalized by that at σ_{bo} of 0.45.

4. Experimental Results

To confirm the performance of DSI and the PSM, exposure tests were conducted using a test exposure tool for 6" wafers. The resist used in the tests was a prototype for DUV exposure provided by Tokyo Ohka Kogyo Co., Ltd. A test Att. PSM and BIM for 6" wafers manufactured by SK-Electronics Co., Ltd. were used. The wavelength of the no-phase error was configured to a centroid wavelength of 340 nm, and the intensity transmittance of the phase-shifting film was in the range of 5–10% at 340 nm. The design of the illumination sources and exposure spectrum were the same as those of the OAI and DSI (Fig. 2 and Fig. 5). The OAI was formed by inserting an annular aperture into the illumination optics of the exposure tool. In the same way, the DSI was formed by inserting a wavelength filter, which cut off 350–385 nm light at $\sigma = 0.45$–0.65. The exposed pattern was 1.0 μm L/S, and the DOF was evaluated to be a 10% variation of the bottom CD of 1.0 μm.

Figure 12 shows the experimental results of the DSI and OAI with a PSM and BIM. As evident, the resist profile for OAI and the BIM was not resolved sharply, while that for DSI and the BIM resolved while retaining the top of the resist, indicating that the DSI improved the resolution. The PSM appears to be more efficient for improving the resolution; however, the DOF for OAI and the PSM was insufficient, with a value of 19.5 μm. The DOF for DSI and the PSM was 25.1 μm, indicating that DSI improved the DOF by approximately 30%. Note that the DOF for a 1.0 μm L/S with DSI and the PSM was larger than that for a 1.2 μm L/S pattern with OAI and the BIM, i.e., 24.3 μm (as mentioned in Sect. 1). Thus, the combination of the DSI and PSM was effective for resolving 1.0 μm L/S with sufficient DOF.

5. Discussion

This study primarily aimed to develop a technique to resolve 1.0 μm L/S with sufficient DOF. Experimental results demonstrated that the DSI and PSM could resolve a 1.0 μm L/S pattern with a large DOF—larger than that of a 1.2 μm L/S with OAI and a BIM. Therefore, we concluded that DSI and a PSM are practical solutions for achieving 1.0 μm L/S resolution for FPD manufacturing.

Owing to the requirements of higher throughput, exposure tools for FPD manufacturing have enlarged the exposure regions as well as masks and glass plates. This trend has resulted in diminished focus control. Because small CDs tend to increase this difficulty, a technique to obtain sufficient DOF is essential for future high-resolution processes. To achieve both high resolution and large DOF, the standard strategies for improving resolution—enlarging the NA and shortening the exposure wavelength—cannot be easily applied because they decrease the DOF. In addition, such modifications require new developments concerning light sources, optical filters, deposition control methods, and larger optical elements, which incur high development

costs.

RETs, such as DSI and PSMs, may solve these issues. Even though the use of such RETs does not require modifications of the NA and λ, both the resolution and DOF are significantly improved. This study and our recent research have demonstrated that an Att. PSM—usually utilized with narrowband illumination—is also effective for broadband illumination. Furthermore, the new illumination technique, DSI, was shown to be sufficiently effective, even in conjunction with a PSM in broadband illumination.

For practical use of DSI and a PSM, we plan to investigate the impact of aberration. It is known that optimizing the illumination source generally increases the sensitivity to aberration of projection optics [30]. Because the experimental results of this study were obtained at one image height with the test exposure tool for a 6” wafer, the influence of aberration and the performance uniformity across the exposure area needs to be investigated using an exposure tool with larger glass plates.

In addition, a technique to compensate for the exposure time is needed. The DSI formed by a wavelength filter reduces the illumination intensity. Furthermore, a PSM requires a higher dose compared to that of a BIM. Both factors have a negative influence on the exposure time, lowering throughput. Thus, DSI formation without illumination loss could be the subject of further research in this direction for improved practical applications.

6. Conclusions

In this paper, we investigated RETs with 1.0 μm L/S resolution and sufficient DOF for FPD lithography applied in broadband illumination. To this end, we proposed to combine the previously developed RET, DSI, with an Att. PSM. Theoretical observations and computer simulations were used to arrive at a method to design the parameters of an Att. PSM for broadband illumination. We proposed that the transmittance of a phase-shifting film should be determined to increase contrast and reduce resist loss. The wavelength at which the light undergoes 180° phase-shift should be determined around the centroid wavelength of the illumination spectrum for enhancing image intensity. It was also confirmed that the DSI is effective for enhancing DOF even in conjugation with an Att. PSM. Experimental results demonstrated that DSI and PSM could resolve 1.0 μm L/S with a large DOF, which even surpasses that of 1.2 μm L/S.

Although using such techniques to improve resolution could potentially introduce some problems, our approach is valid for achieving resolution up to 1.0 μm L/S in FPD lithography. Our technique has the potential to be indispensable for manufacturing future high-end display devices.

Acknowledgments

The authors would like to thank Asahi Spectra Co., Ltd. for providing optical filters, SK-Electronics Co., Ltd. for providing the PSM, and TOKYO OHKA KOGYO CO., LTD for providing the resist. We would like to thank Editage for English language editing. We also thank Nozomu Izumi and Miwako Ando for their technical assistance and meaningful discussions regarding the experiments.

References

[1] T. Ito and S. Okazaki, “Pushing the limits of lithography,” Nature, vol.406, pp.1027–1031, 2000.
[2] J.H. Bruning, “Optical lithography: 40 years and holding,” Proc. SPIE 6520, Optical Microlithography XX, 652004, 2007.
[3] J. Dyson, “Unit magnification optical system without Seidel aberrations,” J. Opt. Soc. Am., vol.49, no.7, pp.713–716, 1959.
[4] A. Offner, “New concepts in projection mask aligners,” Opt. Eng., vol.14, no.2, 142130, pp.130–132, 1975.
[5] A. Suzuki, “Complete analysis of a two-mirror unit magnification system. Part 1,” Applied Optics, vol.22, no.24, pp.3943–3949, 1983.
[6] M. Kohno, K. Fukami, H. Yoshioka, S. Watanabe, and A. Suzuki, “Catadioptric projection optical system for flat panel exposure tool,” Proc. SPIE 6342, International Optical Design Conference 2006, 2006.
[7] L. Rayleigh, “On the theory of optical images, with special reference to the microscope,” The London, Edinburgh, and Dublin Philosophical Magazine and Journal of Science, vol.42, no.255, pp.167–195, 1896.
[8] K. Nagano, N. Yabu, M. Hakko, M. Ando, N. Izumi, and Y. Osaki, “Development of G6 exposure tool for 1.2 μm resolution,” J. Soc. Inf. Display, vol.27, no.5, pp.265–272, 2019.
[9] P.E. Malinowski, T. Ke, A. Nakamura, P. Vicca, A.J. Kronemeijer, M. Ameys, J.L. van der Steen, S. Steudel, Y. Kamochi, Y. Iwai, G. Gelinck, and P. Heremans, “Photolithography as enabler of AMOLED displays beyond 1000 ppi,” SID Symposium Digest of Technical Papers, vol.48, no.1, pp.623–626, 2017.
[10] C.A. Annis, “Roadmapping strategies for rapidly diversifying FPD applications and manufacturing technologies,” SID Symposium Digest of Technical Papers, vol.50, no.1, pp.762–764, 2019.
[11] K. Suzuki, M. Hakko, M. Ando, K. Takasaki, N. Yabu, K. Nagano, and N. Izumi, “High resolution technologies of 1.0 μm L/S using PSM specialized in DUV broadband illumination,” Proc. IDW ’19, pp.713–716, 2019.
[12] M. Hakko and K. Suzuki, “Resolution enhancement with source-wavelength optimization according to illumination angle in optical lithography,” J. Micro/Nanolithogr. MEMS MOEMS, vol.19, no.4, 043201, 2020.
[13] C.A. Mack, “Optimum stepper performance through image manipulation,” Proc. KTI Microelectronics Seminar, Interface, pp.209–215, 1989.
[14] A.K.-K. Wong, Resolution enhancement techniques in optical lithography, SPIE, Washington DC, 2001.
[15] M. Noguchi, M. Muraki, Y. Iwasaki, and A. Suzuki, “Subhalf-micron lithography system with phase-shifting effect,” Proc. SPIE 1674, Optical/Laser Microlithography V, pp.92–104, 1992.
[16] N. Shiraishi, S. Hirukawa, Y. Takeuchi, and N. Magome, “New imaging technique for 64M-DRAM,” Proc. SPIE 1674, Optical/Laser Microlithography V, pp.741–752, 1992.
[17] D.L. Fehrs, H.B. Lovering, and R.T. Scruton, “Illuminator modification of an optical aligner,” Proc. KTI Microelectronics Seminar, pp.217–230, 1989.
[18] C.A. Mack, “Optimization of the spatial properties of illumination for improved lithographic response,” Proc. SPIE 1927, Optical/Laser Microlithography, pp.125–136, 1993.
[19] M.D. Levenson, N.S. Viswanathan, and R.A. Simpson, “Improving resolution in photolithography with a phase-shifting mask,” IEEE Trans. Electron Devices, vol.29, no.12, pp.1828–1836, 1982.
[20] M.D. Levenson, D.S. Goodman, S. Lindsey, P.W. Bayer, and H.A.E. Santini, “The phase-shifting mask II: Imaging simulations and sub-

micrometer resist exposures," IEEE Trans. Electron Devices, vol.31, no.6, pp.753–763, 1984.
[21] B.J. Lin, "The attenuated phase-shifting mask," Solid State Technol., vol.35, no.1, pp.43–47, 1992.
[22] T. Terasawa, N. Hasegawa, H. Fukuda, and S. Katagiri, "Imaging characteristics of multi-phase-shifting and halftone phase-shifting masks," Jpn. J. Appl. Phys., vol.30, no.11B, pp.2991–2997, 1991.
[23] T. Ii and M. Otaki, "Development of high-quality attenuated phase-shift masks," Yield Management Solutions, vol.3, no.1, pp.41–45, 2000.
[24] O. Popa and R. Jonckheere, "Attenuated phase shift masks using MoSi as an opaque layer," 1995 International Semiconductor Conference, CAS '95 Proceedings, pp.171–174, 1995.
[25] M. Hakko, N. Yabu, M. Ando, N. Izumi, and K. Nagano, "To specialize an attenuated phase shift mask in DUV broadband illumination," Proc. IDW '17, pp.577–580, 2017.
[26] C.A. Mack, Fundamental principles of optical lithography: The science of microfabrication, Wiley, England, 2007.
[27] L. Straaijer, "Formulas for lithographic parameters when printing isolated and dense lines," J. Micro/Nanolithogr. MEMS MOEMS, vol.4, no.4, 043001, 2005.
[28] C.A. Mack, "PROLITH: A comprehensive optical lithography model," Proc. SPIE 0538, Optical Microlithography IV, pp.207–220, 1985.
[29] C.A. Mack, M.D. Smith, and T. Graves, "The impact of attenuated phase shift mask topography on hyper-NA lithography," Proc. SPIE 5992, 25th Annual BACUS Symposium on Photomask Technology, 59920Z, 2005.
[30] T.A. Brunner, "Impact of lens aberrations on optical lithography," IBM J. Res. Develop., vol.41, no.1/2, pp.57–67, 1997.

Kanji Suzuki obtained a Bachelor's degree in science and a Master's degree in physics from Kyoto University (Japan) in 2015 and 2017, respectively. He joined Canon Inc. in 2017 and is now an engineer in the FPD production equipment design division of Canon Inc.

Manabu Hakko obtained a Bachelor's degree in science and a Master's degree in physics from Keio University (Japan) in 2001 and 2003, respectively. He joined Canon Inc. in 2003. He also earned a Ph.D. degree in physics from Utsunomiya University in 2014. He is now an engineer in the FPD production equipment design division of Canon Inc.